Journal of Medicinal and Nanomaterials Chemistry 3 (2023) 199-212

Journal of Medicinal and Nanomaterials Chemistry

Journal homepage: https://jmnc.samipubco.com/

Original Research Article

Enhanced physical properties of SnS/SnO semiconductor material

Egwunyenga Nkechi Josephine[1,2], Okunzuwa Samuel Ikponmwosa[2], Thamer Alomayri[3], Imosobomeh Lucky Ikhioya[4,5] *

[1] *Department of Science Laboratory Technology, Delta State Polytechnic Ogwashi-Uku, Nigeria*
[2] *Department of Physics, University of Benin, Benin City, Nigeria*
[3] *Department of Physics, Faculty of Applied Sciences, Umm Al-Quar University, Makkah, Saudi Arabia*
[4] *Department of Physics and Astronomy, University of Nigeria, Nsukka, Enugu State, Nigeria*
[5] *National Centre for Physics, Quaid-i-Azam University Campus, Islamabad, Pakistan*

ARTICLE INFORMATION

Received: 23 June 2023
Received in revised: 15 August 2023
Accepted: 19 August 2023
Available online: 20 August 2023
Checked for Plagiarism: **YES**

DOI: 10.48309/JMNC.2023.3.3

KEYWORDS

Bandgap
Tin sulphide
SILAR
SEM
EDX
XRD

ABSTRACT

This research aims at characterizing SnS/SnO material for photovoltaic applications where the molar concentration of tin (Sn) varied as the parameters for characterization in the synthesis's process from 0.1-0.4 mol *via* the successive ionic layer adsorption reaction (SILAR) approach. A face-centered cubic structure with orientations along the 200 plane corresponds to the considerable peak at 2theta values of 31.82°. The lattice constant rises as the 2-theta angle rise from 20° -70°, causing the material's diffraction peak to become less intense. Crystallites made up of different sizes were found with the film deposited with 0.1 mol of tin, comprising unevenly shaped rods and loosely packed particles, whereas at 0.2 mol, the crystallite size is more sizable than the materials deposited at 0.3 mol to 0.4 mol and gets smaller as the molarity level rises. The thickness of the material rose from 109.12 to 112.21 nm, which caused the resistivity of the deposited material to decrease from 9.562×10^{9} -7.312×10^{9}. The electrical conductivities of the deposited SnS/SnO material increased proportionally to the thickness of the material with values between (1.045-1.367) x 10^{-10}.

Corresponding author, email: imosobomeh.ikhioya@unn.edu.ng, nkeopene@gmail.com (I.L. Ikhioya).

Graphical Abstract

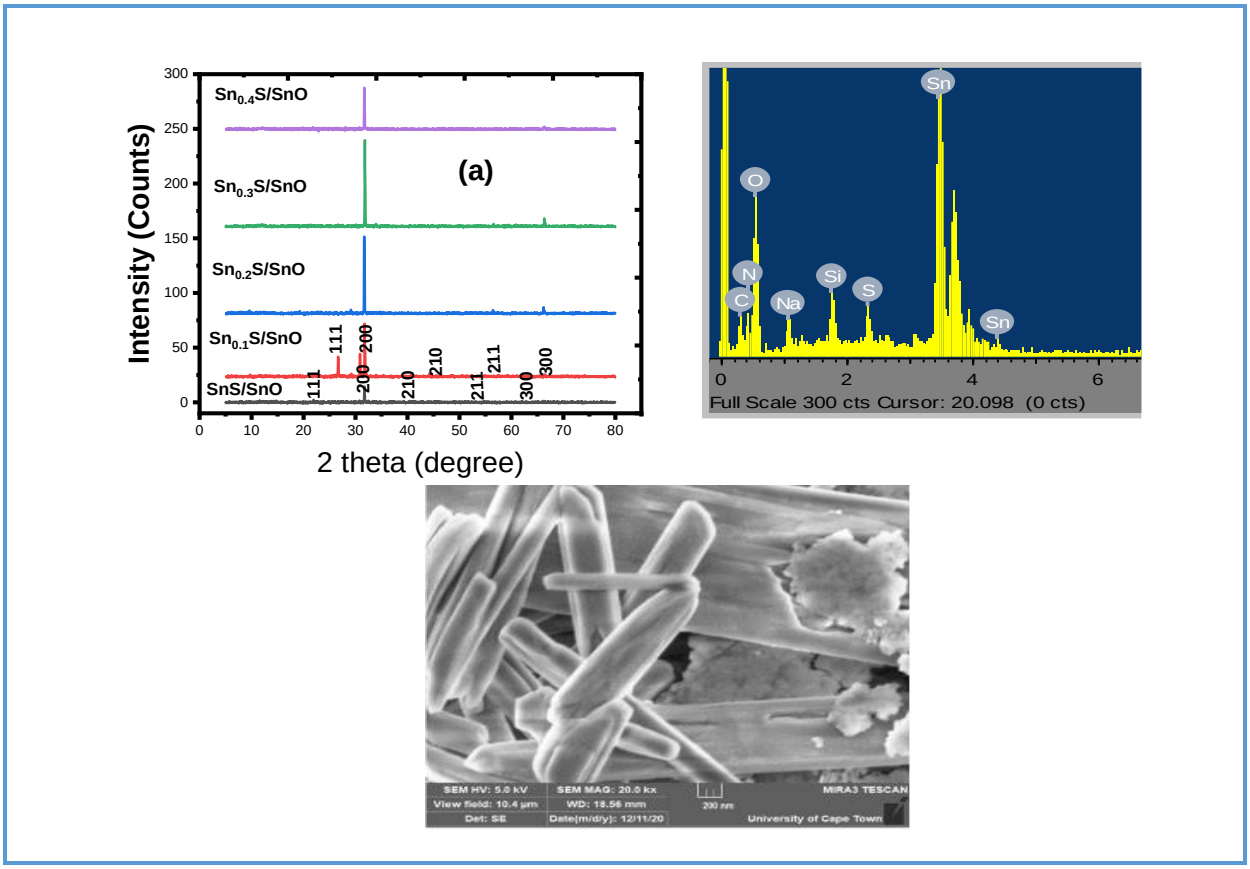

Introduction

The development rate caused a rapid increase in the requirement for energy in homes and industries. The energy was primarily obtained from fossil fuels like crude oil, wood, coal, and gas [1-7]. These fossils are composed of biological organisms that lived and died millions of years ago [8-9]. The remains of dead biological matter were transported deep beneath the earth's surface and, through high heat and pressure, transformed into fossil fuels. Multiple efforts are being made to meet the rising energy requirements, and nuclear energy is considered a primary option for generating electricity with minimal carbon emissions [10-12]. There are uncertainties in nuclear fuel reserves, reactor efficiency with lower-grade uranium ores, and nuclear waste disposal solutions. Solar energy has many uses and can be harnessed in many ways. Photochemical, photoelectrical, and photothermal conversion are included. Life on Earth depends on photosynthesis as the primary mechanism. Thermal energy is produced from solar radiation using heating components in solar thermal systems [13-22]. The conversion of solar energy to electrical energy occurs directly through photovoltaic cells in the photoelectrical process. PV cells are being studied to make energy generation more efficient and cheaper. Solar energy scientists face severe difficulty meeting most of the world's energy needs with PVs, partly because current PV production is minimal compared to fossil fuel-based power [23-29]. In essence, researchers were drawn to the development of thin films for the generation of Solar power has been suggested as a viable

future alternative energy source. [30-33]. Tin oxide/sulfide (SnS/SnO) has intriguing physical and chemical characteristics. Applications in optoelectronics have been triggered [18]. It is utilized in electrochemical capacitors and as electrode materials [19]. Catalysts, rechargeable batteries, [20]. Devices with magneto electronics [21]. Magnetic oxide perovskite compounds, which exhibit a wide range of electrical and magnetic features, such as metal-insulator transistors and massive magneto-resistance, were created using SnO as a substrate [22].

SnS is an innovative component for solar cells. Due to SnS's high optical absorption and energy bandgap of around 1.3 eV, The bulk of the incident light can be absorbed with as little as a few microns of SnS. In addition to being composed of plentiful, ecologically friendly materials, SnS is also amphoteric, allowing for versatility in device design. Examples of structures that can be envisaged include p-i-n structure, p-n junction made of SnS with an SnS-based i-layer, and heterojunction devices with an n-type window layer and p-type SnS absorber layer. These and other encouraging findings imply the relatively high likelihood of developing devices with efficiency > 10%. SnS-based thin film solar cell devices have now been made with more than 2 % efficiency. In the industry, layers of tin are frequently deposited on substrates with enormous surfaces and well-established industrial subsidization techniques; in comparison to the existing widely used copper indium gallium diselenide and cadmium telluride thin technologies, industrializing this technique should be simpler [34]. Numerous techniques, including spray pyrolysis [35], chemical bath deposition [36], successive ionic layer adsorption and reaction (SILAR) [37], electron beam evaporation [38], and chemical vapor deposition [39], have been used to create tin oxide films. Physical techniques like sputtering yield highly resistive coatings, but chemical techniques have been shown to produce less resistive films. The SILAR approach is practical for duplicating films and is simple and affordable [40]. The substrates are alternately dipped into aqueous solutions of component ions during controlled deposition cycles. By using the SILAR process for solar energy application, it is truly possible to fabricate ecologically friendly tin oxide and sulphide are examples of semiconductor materials. The semiconductor SnS, which is a member of the IV-VI group, has an energy bandgap of 1.3 eV and a high absorption, making it a strong option for an absorption layer.

One of the most widely used transparent conducting oxides and an excellent material for window or buffer layers in heterojunction solar energy applications is SnO, which has a broadband gap of 3.8 eV [10]. Tin oxide has been widely used in many optical electronics, such as light-emitting diodes, electrode and buffer layer materials in solar cells, and transparent-filled effect transistors due to its low electrical resistance and good optical transparency in the visible range and good thermal resistance [18], and it is considered one of the most significant n-type semiconductors, tin oxide (SnO) [22].

Raj *et al*. (2018) [21] used the successive ionic layer adsorption reaction (SILAR) approach to uniformly deposit tin oxide thin films onto a glass substrate while employing diamine as a complexing agent. The deposited films had an energy band gap of about 3.85 eV and an electrical conductivity ranging from 4.23 x 108 Ωcm to 11.83 x 108 Ωcm.

The CdS/SnS heterojunction currently has the maximum solar conversion efficiency of 1.3 % in heterojunction devices using SnS. SnS/SnO, however, have a benefit for solar energy applications because their constituent

elements are generally cheap, plentiful, and harmless. However, SnS partners in SnO heterojunction to prevent CdS layer toxicity. Combining chemical bath deposition and spray pyrolysis procedures, Ristov *et al*. (2001) [20] created an SnS/F: SnO_2 heterostructure. As a result, this study evaluates and reports on the fabrication of SnS/SnO heterojunction thin films by the SILAR process with molar (concentration) modification for photovoltaic application.

The research involved varying the molar concentration of tin (Sn) within the range of 0.1-0.4 mol precursor pH 7.0 while keeping all other parameters constant to understand its role in the synthesis process. The objective is to investigate the impact of tin's molar concentration on the synthesized material for photovoltaic application.

In this article, we describe the structural, optical, electrical, and elemental composition of SnS/SnO material, which was synthesized using a straightforward, inexpensive successive ionic layer adsorption reaction (SILAR) approach with anticipation that SnS/SnO material will be combined to create novel functional materials for use in photovoltaic applications.

Experimental procedure

The following precursors were employed in the deposition of SnS/SnO: The cationic precursor solution was made using 0.01 mol of tin (II) chloride dihydrate ($SnCl_2.2H_2O$), and the anionic precursor solution was made using 0.01 mol of thioacetamide (C_2H_5NS). Four 50 mL beakers containing tin (II) chloride dihydrate ($SnCl_2.2H_2O$) solution. Distilled water and Thioacetamide (C_2H_5NS)/potassium hydroxide (KOH) solution. A well-cleaned glass substrate that had been washed with acetone, distilled water, and acid was submerged in a cationic precursor solution of tin (II) chloride dihydrate ($SnCl_2.2H_2O$) for 10 s to allow tin ions to adhere to the surface of the substrate. The substrate was washed in distilled water to remove the loosely attached Sn2+ ions for 5 seconds. The substrate was then submerged in the Thioacetamide (C_2H_5NS)/potassium hydroxide (KOH) anionic precursor solution for 10 seconds to create a layer of SnS/SnO materials. One SILAR cycle of SnS deposition was finished by rinsing the substrate in distilled water for 5 s to remove the unreached species. The molar concentration of tin (Sn) varied as the parameters for characterization in the process of the synthesis from (0.1- 0.4) mol precursor pH 7.0, and precursor temperature (room) and every other parameter were kept constant. The synthesis of SnS/SnO films, tin oxide (SnO) was first deposited on the glass substrate dry in the oven for 30 min, and tin sulphide (SnS) was deposited on the grown SnO films to make SnS/SnO films, and it was repeated for a different parameter for characterization.

Characterization Techniques

The characterization of the deposited films was ascertained using some currently in-use techniques. Knowing the chemical composition, crystal structure, crystallite size, surface morphology, band gap energy, optical absorption, transmittance, and absorbance of the formed film is possible thanks to characterization. Phase identification of the films by X-ray diffraction was used to determine the chemical compositions of the thin films produced in this work using a scanning electron microscope (SEM) model A-VPSE G3 with an acceleration voltage of 20 kV and a magnification range of 200x to 1000x, the morphology and size of the prepared particles were investigated. The optical characteristics of the deposited films were examined for their absorbance and transmittance at normal

incidence using a UV-visible spectrophotometer, model number 756S.

Results and Discussion

XRD result analysis

Figure 1a shows the XRD patterns of the SnS/SnO coated on a glass substrate at different concentrations. At 2 theta values of 31.82°, a significant peak was found, and this value corresponds to the face-centered cubic crystal structure with orientations along the (200) plane. The glass substrates used for the deposition may have contributed to the unindexed peaks. According to Table 1, the lattice constant rises as the 2-theta angle rises from 20° -70°, causing the material's diffraction peak to become less intense. The Debye-Scherrer equation was used to calculate the average crystallite sizes based on the diffraction peaks' full width at half maximum (FWHM). The XRD pattern revealed that the films were polycrystalline [31].

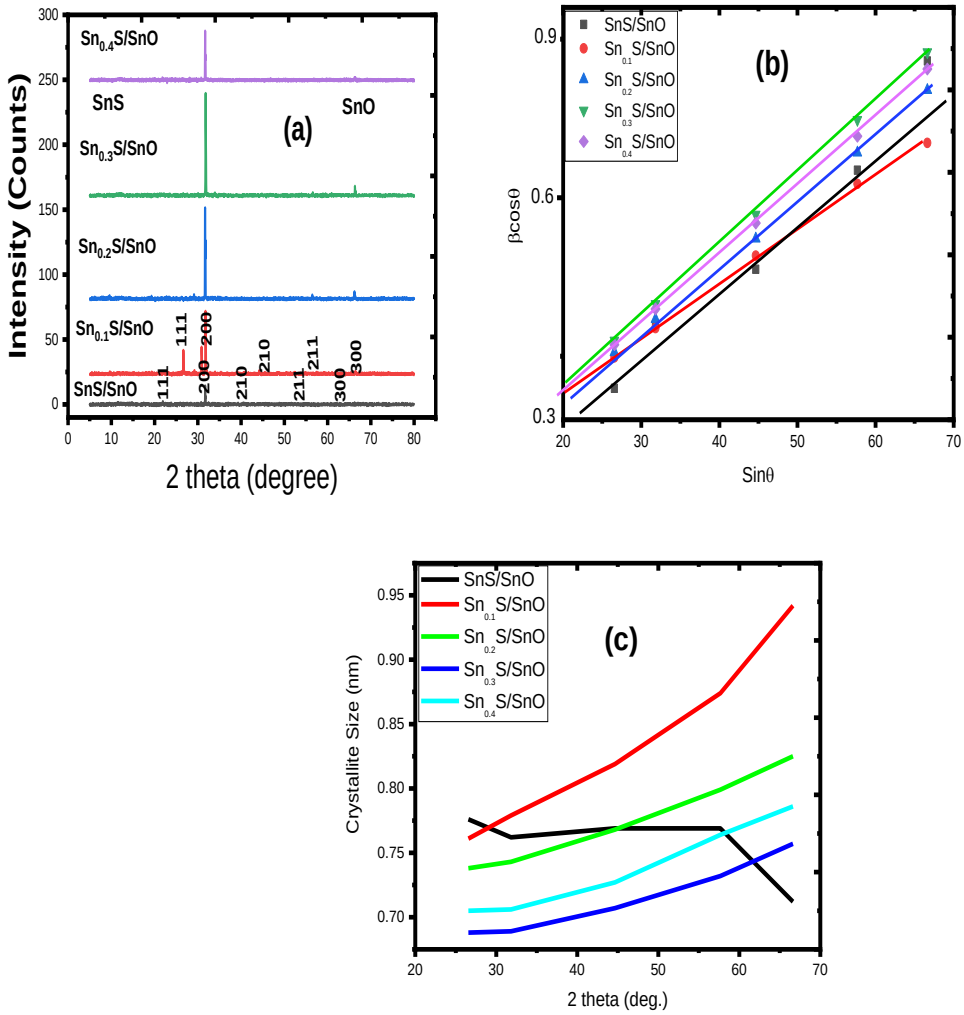

Figure 1. (a) XRD pattern (b) Williamson Hall plot (c) Crystallite size *vs.* 2 theta plot of SnS/SnO material deposited at different molar percentage concentrations

Table 1. Structural values for the SnS/SnO

Films	2θ (degree)	d(Å)	(Å)	β	Hkl	D (nm)	δ m^2
SnS/SnO	21.93	4.049	7.013	0.182	111	0.776	5.155
	31.82	2.809	5.619	0.189	200	0.762	5.550
	40.33	2.234	4.468	0.192	210	0.769	5.715
	53.79	1.702	3.807	0.202	211	0.769	6.291
	62.77	1.478	3.622	0.228	300	0.712	7.824
$Sn_{0.1}S/SnO$	26.56	3.352	5.807	0.187	111	0.761	5.124
	31.82	2.809	5.619	0.185	200	0.779	4.640
	44.66	2.027	4.054	0.183	210	0.819	4.072
	57.67	1.596	3.570	0.181	211	0.874	3.625
	66.63	1.402	3.434	0.176	300	0.942	4.662
$Sn_{0.2}S/SnO$	26.56	3.352	5.807	0.193	111	0.738	5.458
	31.82	2.809	5.619	0.194	200	0.743	5.102
	44.66	2.027	4.054	0.195	210	0.768	4.623
	57.67	1.596	3.570	0.198	211	0.799	4.337
	66.63	1.402	3.434	0.201	300	0.825	6.080
$Sn_{0.3}S/SnO$	26.56	3.352	5.807	0.207	111	0.688	6.279
	31.82	2.809	5.619	0.209	200	0.689	5.922
	44.66	2.027	4.054	0.212	210	0.707	5.464
	57.67	1.596	3.570	0.216	211	0.732	5.162
	66.63	1.402	3.434	0.219	300	0.757	7.218
$Sn_{0.4}S/SnO$	26.56	3.352	5.807	0.202	111	0.705	5.979
	31.82	2.809	5.619	0.204	200	0.706	5.642
	44.66	2.027	4.054	0.206	210	0.727	5.159
	57.67	1.596	3.570	0.207	211	0.764	4.741
	66.63	1.402	3.434	0.211	300	0.786	6.701

Results from the XRD are used to plot the Williamson-Hall plot (β cos θ against Sin θ) in Figure 1b. Williamson Hall plot's slope rises as the tin molar concentration does [30]. As a result of strain hardening, the dislocation density increases and the grain size decreases for the SnS/SnO and increase as the tin molar concentration increases, increasing the prominent peak of the diffraction angle. Figure 1c reveals a plot of the grain size of the deposited material *vs*. 2-theta diffraction angle. The graph showed that the SnS/SnO material changes as the diffraction angle rises, in contrast to the tin molar concentration-dependent variation of the material. As the diffraction angle increases, the crystallite size increases.

Surface Morphological Analysis

SEM was used to evaluate the size and distribution of the particles during the deposition of thin film materials in Figure 2. The surface morphological image of all the deposited components (SnS/SnO) is visible at a 200 nm magnification. Figure 2a depicts the discovery of various-sized crystallites of tiny rods and loosely packed particles. As the molarity level rises, the size of the crystallite decreases, starting at 0.2 mol, compared to the materials deposited at 0.3 mol to 0.4 mol [31, 36]. The films show how the aggregation of the particles resulted from the growth of SnS/SnO material. The elemental makeup of the SnS/SnO compound was identified using electron dispersive X-ray spectroscopy, as seen in Figure 3. The positions of the peaks in a typical EDX spectrum show the existence of the essential elements, and the peak height measures the concentration of each element in the film samples. The EDX results of the films show that tin, oxygen, and sulfur are all present, with a more significant intensity peak for tin and oxygen and evidence of sulfur's existence. Due to the elemental composition of the substrate utilized in the deposition, other elements like sodium (Na), carbon (C), silicon (Si), and nitrogen (N) are also present (see Table 2 for details). [14].

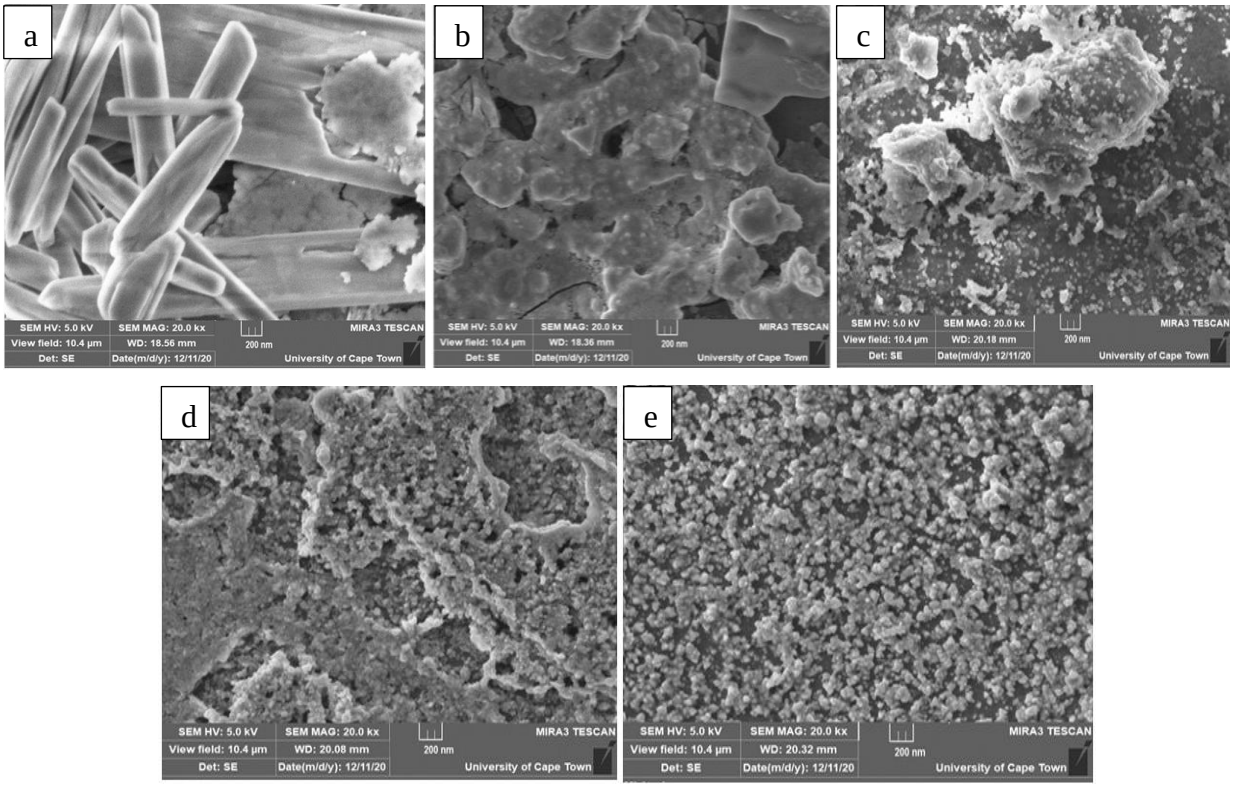

Figure 2. SEM micrograph of (a) SnS/SnO, (b) $Sn_{0.1}S/SnO$, (c) $Sn_{0.2}S/SnO$, (d) $Sn_{0.3}S/SnO$, (e) $Sn_{0.4}S/SnO$

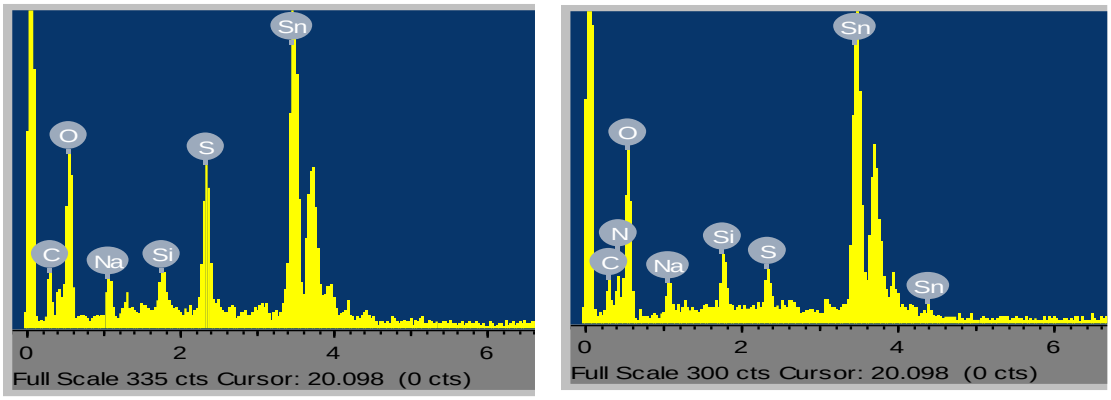

Figure 3. EDX spectrum

Table 2. Constituent element's atomic percentage weight

SnS/SnO		**$Sn_{0.1}S$/SnO**	
Elements	A.W (%)	Elements	A.W (%)
O	19.18	O	15.0
S	15.02	S	10.0
Si	10.0	Si	12.7
C	2.60	C	1.0
Na	2.00	Na	2.0
Sn	51.20	Sn	51.0
-	-	Sn	7.1
-	-	N	2.2

Electrical Study

Table 3, information on the electrical characteristics of the tin sulphide/tin oxide material, demonstrates that the material was deposited at various concentrations of 0.1 - 0.4 mol. As the material's concentration increased, the material's thickness rose from 109.12 to 112.21 nm, which caused the resistivity of the deposited material to decrease from 9.562×10^{9} -7.312×10^{9}. The electrical conductivities of the deposited SnS/SnO material increased proportionally to the thickness of the material with values between (1.045-1.367) x 10^{-10} [31].

Table 3. Electrical properties of SnS/SnO

Films	**t(nm)**	**ρ (Ω.cm)**	**σ $(Ω.cm)^{-1}$**
SnS/SnO	109.12	9.562 x 10^{9}	1.045 x 10^{-10}
$Sn_{0.1}S$/SnO	110.01	8.672 x 10^{9}	1.153 x 10^{-10}
$Sn_{0.2}S$/SnO	110.23	8.342 x 10^{9}	1.198 x 10^{-10}
$Sn_{0.3}S$/SnO	111.02	7.435 x 10^{9}	1.344 x 10^{-10}
$Sn_{0.4}S$/SnO	112.21	7.312 x 10^{9}	1.367 x 10^{-10}

Optical Study

As the wavelength increases, it can be seen in Figure 4a that the film's absorbance varies. The absorbance is also altered as a function of concentration. The SnS/SnO films and 0.1 mol of Sn ion have a relatively constant absorbance value over the spectral range. The absorbance values increased to peak levels in the UV spectrum in the films deposited with 0.2 and 0.3 mol, and 0.4 mol. There was an exponential decline in absorbance in the VIS and INR regions [31]. The results also showed that the absorbance of the films increased as the Sn ion concentration increased for films deposited with 0.2-0.4 mol, respectively. As the wavelength increases, it was found that the films' transmittance fluctuates, as seen in Figure 4b. The Sn ion concentration also influenced the % transmittance. The transmittance values of the films produced with 0.2 mol of Sn ion and without Sn concentration fluctuate somewhat over the whole spectral range. The transmittance values of films made with 0.3 mol, 0.4 mol, and 0.5 mol in the UV spectra reached their lowest points. The transmittance sharply increased toward the VIS and INR zones. The outcomes also showed that the % transmittance of the films dropped as the Sn ion concentration increased for films deposited with 0.2 and 0.3 mol and 0.4 mol, respectively. The reflectance values of the films in Figure 4c revealed that they were not highly reflective [31]. The reflectance of the deposited films ranged from 0.34 to 20.30 %. Films deposited without Sn concentration and with 0.2 mol of Sn ion have similar patterns, but films deposited with 0.3, 0.4, and 0.5 mol of Sn ion have similar patterns with peaks emerging at varied wavelengths. These differences in the reflectance values of the deposited films suggested that they might be applied as anti-reflective coatings.

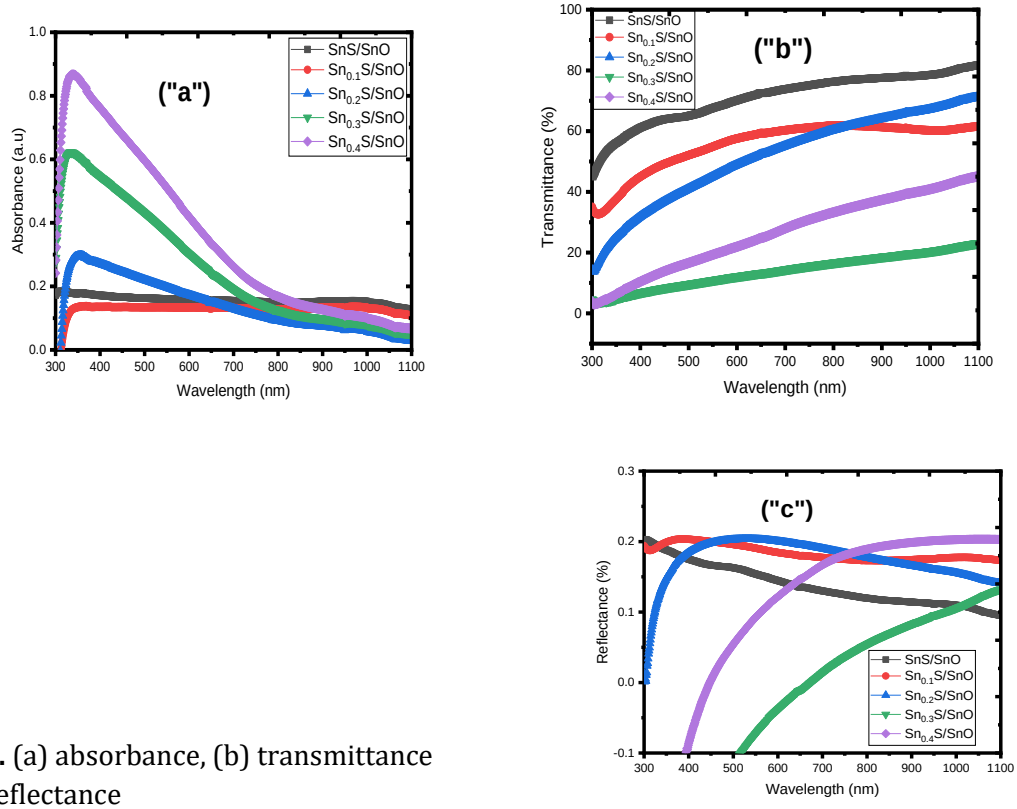

Figure 4. (a) absorbance, (b) transmittance and (c) reflectance

The energy bandgap plot of the deposited SnS/SnO films is depicted in Figure 5 and was estimated using the Tauc equation: $(\propto hv)^2 = A(hv - E_g)$ 1.35 eV is the band gap determined from the films without Sn concentration. It was found that the film synthesized with Sn concentration had a bandgap energy of 1.25 eV – 1.51 eV [31].

The films' refractive indices ranged from 1.12 to 2.64, as depicted in Figure 6a. Films made with 0.1 mol of Sn ion and without Sn concentration have a similar pattern in their refractive indices, whereas those made with 0.2, 0.3, and 0.4 mol of Sn ion do not. Figure 6b illustrates how the extinction coefficient of the films changed as photon energy rose. The extinction coefficient was also impacted by concentration. Films made with 0.1 mol of Sn ion but no Sn concentration exhibit a slight variation in extinction coefficient value in the spectral region. The films deposited using 0.2, 0.3, and 0.4 mol reached peak extinction coefficient values in the UV spectrum. The extinction coeff. Decreased steadily toward the VIS and INR zones. The outcomes also demonstrated that the extinction coeff.

Of the films climbed as the Sn ion concentration increased for films deposited with 0.2, 0.3, and 0.4 mol, respectively. These films' extinction coefficient in the VIS and NIR region is slightly lower than values obtained for films deposited with 0.1 mol/L Sn and zero Sn concentration [31]. Figure 6c illustrates how the optical cond. values of the films declined as photon energy rose. The graph also showed that the optical cond. of the films rose as Sn ion concentration did. In the UV range, peak optical conductivity values were observed. This demonstrated that the deposited layers allowed more UV radiation to pass through as compared to VIS and NIR photons.

The range of the films' actual dielectric constant values, as shown in Figure 7a, was between 0.5 and 0.77. While films deposited with 0.2, 0.3, and 0.4 mol of Sn ion have similar patterns with peaks occurring at various photon energy levels, films formed without Sn concentration and 0.1 mol of Sn ion have similar patterns with peaks at different photon energy levels.

The imaginary dielectric const. of the films was found to change as photon energy increased, as seen in Figure 7b. Additionally affected by concentration was the imaginary dielectric const.. The value of the imaginary dielectric const. varies slightly over the spectra range in films formed without Sn concentration and with 0.1 mol of Sn ion.

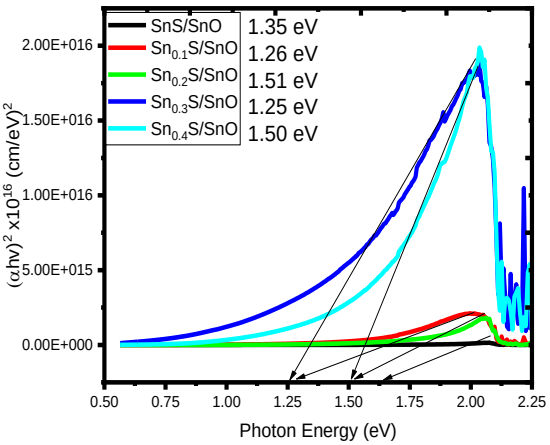

Figure 5. Energy bandgap

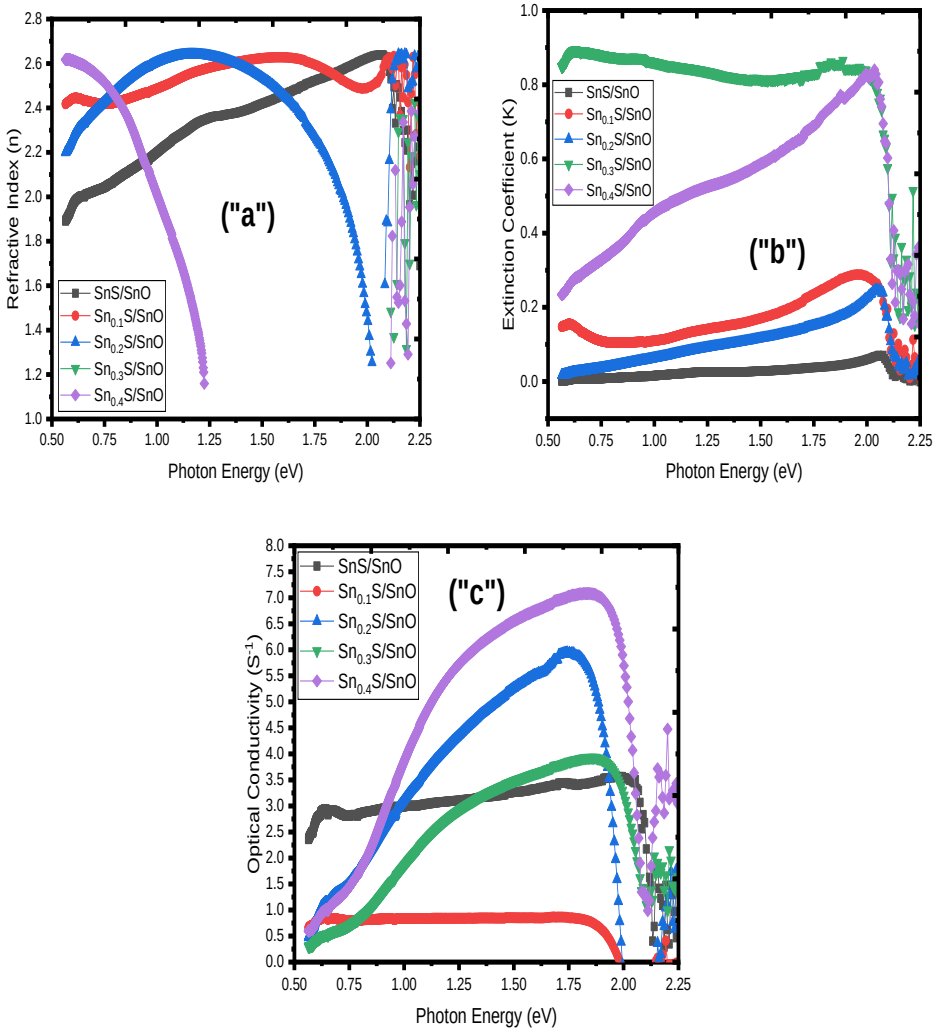

Figure 6. (a) refractive index, (b) extinction coefficient and (c) optical conductivity

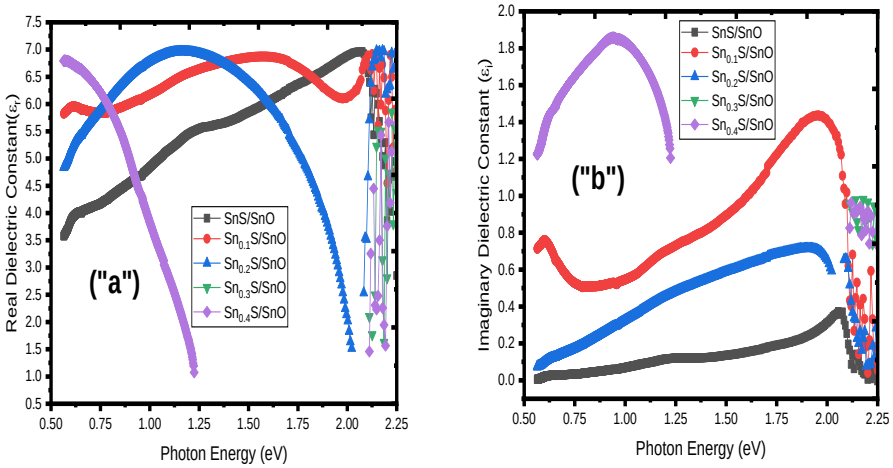

Figure 7. (a) real dielectric and (b) imaginary dielectric constant

The imaginary dielectric constant values in the films deposited at 0.2, 0.3, and 0.5 mol climbed to peak values in the UV spectra. In the direction of the VIS and INR zones, the imaginary dielectric const. continuously dropped. The outcome also showed that for films deposited with 0.2, 0.3, and 0.4 mol, respectively, an increase in the imaginary dielectric constant of the films was seen as the Sn ion concentration rose [31]. These films' imaginary dielectric const. is marginally less than those obtained for films deposited without Sn concentration and 0.1 mol in the VIS and NIR regions.

Conclusion

We have successfully synthesized SnS/SnO material *via* the SILAR method. At 2 theta values of 31.82^{o}, a significant peak was found, and this value corresponds to the face-centered cubic crystal structure with orientations along the (200) plane. The glass substrates used for the deposition may have contributed to the unindexed peaks. The lattice constant rises as the 2-theta angle rise from 20^{o} -70^{o}, causing the material's diffraction peak to become less intense. The surface morphological image of all the deposited components (SnS/SnO) is visible at a 200 nm magnification. SEM image depicts the discovery of various-sized crystallites consisting of tiny rods and loosely packed particles. As the molarity level rises, the size of the crystallite decreases, starting at 0.2 mol, compared to the materials deposited at 0.3 mol to 0.4 mol. The thickness of the material rose from 109.12 to 112.21 nm, which caused the resistivity of the deposited material to decrease from 9.562 × 10^{9} -7.312 × 10^{9}. The electrical conductivities of the deposited SnS/SnO material increased proportionally to the thickness of the material with values between (1.045 -1.367) x 10^{-10}. The transmittance values of the films produced with 0.2 mol of Sn ion and without Sn concentration fluctuate somewhat over the spectral range. The transmittance values of material made with 0.3, 0.4, and 0.5 mol reached their lowest points. The transmittance sharply increased toward the VIS and INR zones.

Acknowledgment

The authors graciously acknowledge the sponsorship of the TETFUND office through institution-based research (IBR).

Disclosure Statement

The authors reaffirm that they are unaware of any personal or financial conflicts that might have appeared to affect the research described in this paper.

Orcid

Imosobomeh L.Ikhioya : 0000-0002-5959-4427

References

[1]. Liu D., Kelly T.L. *Nature Photon.,* 2014, **8**:133 [CrossRef], [Google Scholar], [Publisher]
[2]. Di Z., Tiantian Z., Yu Tian, Xiaolong Z., and Yafang T. *J. Nanomater.,* 2018, **2018**:8148075 [CrossRef], [Google Scholar], [Publisher]
[3]. Lachore W.L., Andoshe D.M., Mekonnen M.A., Hone F.G. *J. Solid State Electrochem.,* 2022, **26**:295 [CrossRef], [Google Scholar], [Publisher]
[4]. Lin Y.C., Chao Y.T. Yao P.C. *Appl. Surf. Sci.,* 2014, **307**:724 [CrossRef], [Google Scholar], [Publisher]
[5]. Taewan K., Jongchul L., Seulki S. *Energies,* 2020, **13**:5572 [CrossRef], [Google Scholar], [Publisher]

[6]. Mahmood K., Sarwar S. Mehran M.T. *Rsc Adv.*, 2017, **7**:17044 [CrossRef], [Google Scholar], [Publisher]
[7]. Oluyamo S.S., Agunbiade D.B. *Int. J. Innov. Res. Adv. Stud*., 2016, **3**:394 [Google Scholar]
[8]. Liu Z., Deng K., Hu J. Li L. *Angew. Chem*., 2019, **58**:11497 [CrossRef], [Google Scholar], [Publisher]
[9]. Ye J., Li Y., Medjahed A.A., Pouget S., Aldakov D., Liu Y., Reiss P. *Small*, 2020, **17**:2005671 [CrossRef], [Google Scholar], [Publisher]
[10]. Zhao O., Ding Y., Cheng D., Zhang J., Hilt F., Rolston N., Jiang G., Dauskardt R.H. *Thin Solid Films*, 2021, **730**:138708 [CrossRef], [Google Scholar], [Publisher]
[11]. Rana C., Bera, S.R., Saha, S. *J Mater Sci: Mater Electron*, 2019, **30**:2016 [CrossRef], [Google Scholar], [Publisher]
[12] Tanusevski A. *Semicond. Sci. Technol*., 2003, **18**:501 [CrossRef], [Google Scholar], [Publisher]
[13]. Patel M., Kim H.S., Kim J. *Nanoscale*, 2017, **9**:15804 [CrossRef], [Google Scholar], [Publisher]
[14]. Azizian-Kalandaragh Y., Khodayari A., Zeng Z, Garoufalis C.S., Baskoutas S., Gontard L.C. *J. Nanopart. Res*., 2013, **15**:1388 [CrossRef], [Google Scholar], [Publisher]
[15]. Zhou B., Li S., Li W. *ACS Appl. Mater. Interfaces*. 2017, **9**:34033 [CrossRef], [Google Scholar], [Publisher]
[16]. Xu Y., Al-Salim N., Tilley R.D. *Nanomaterials*, 2012, **2**:54 [CrossRef], [Google Scholar], [Publisher]
[17]. Obitte, B.C.N., Ikhioya I.L.., Whyte G.M., Chime U.K., Ezekoye B.A., Ekwealor A.B.C., Maaza M., Ezema F.I. *Opt. Mater.*, 2022, **124**:111979 [CrossRef], [Google Scholar], [Publisher]
[18]. Masood M.N., Mohammed N., Husien K.S. *J. Med. Chem. Sci*., 2023, **6**:693 [CrossRef], Google Scholar], [Publisher]
[19]. Reddy K.R., Reddy N.K., Miles R.W., *Sol. Energy Mater. Sol. Cells,*, 2006, **90**:3041 [CrossRef], [Google Scholar], [Publisher]
[20]. Ristov M., Sinadinovski G., Mitreski M., Ristova M. *Sol. Energy Mater. Sol. Cells,* 2001, **69**:17 [CrossRef], [Google Scholar], [Publisher]
[21]. Raj S., Kumar S., Srivastava S.K., Kar P., Poulomi R.P. *J. Nanosci. Nanotechnol.*, 2018, **18**:2569 [CrossRef], [Google Scholar], [Publisher]
[22]. Zou Y., Zhang Y., Hu Y., Gu H. *Sensors*, 2018, **18**:2072 [CrossRef], [Google Scholar], [Publisher]
[23]. Adjibodé S.M., Kassehin C.U., Médégan S.F., Quetin-Leclercq J., Gbaguidi F.A., Poupaert J. *J. Med. Chem. Sci*., 2020, **3**:228 [CrossRef], Google Scholar], [Publisher]
[24]. Li Y., Wang Z., Ren D. *ACS Appl. Energy Mater*., 2019, **2**:3822 [CrossRef], [Google Scholar], [Publisher]
[25]. Tripathi A.M., Mitra S. *RSC Adv*., 2014, **4**:10358[CrossRef], [Google Scholar], [Publisher]
[26]. Ali S., Wang F,, Zafar S., Iqbal T. *IOP Conf. Ser. Mater. Sci. Eng*., 2018, **275**:012007 [Google Scholar]
[27]. Deepa K.G., Nagaraju J. *Mater. Sci. Semicond. Process*., 2014, **27**:649 [CrossRef], [Google Scholar], [Publisher]
[28]. Ghosh B., Das M., Banerjee P., Das S. *Semicond Sci Technol*., 2008, **23**:125013 [Google Scholar]
[29]. Ravuri S., Pandey C.A., Ramchandran R., Jeon S.K., Grace A.N. *Int J Nanosci*., 2018, **17**:1760022 [CrossRef], Google Scholar], [Publisher]

[30]. Dutta S., Chakrabarti M., Chattopadhyay S., Jana D., Sanyal D., Sarkar A., *J. Appl. Phys*., 2005, **98**:053513 [CrossRef], [Google Scholar], [Publisher]
[31]. Josephine, E.N. Ikponmwosa O.S., Ikhioya I.L., *East Eur. J. Phys*. 2023, **1**:154 [CrossRef], Google Scholar], [Publisher]
[32]. Ahmad, F., Mehmood, M. *Adv. J. Chem. A*, 2022, **5**:287 [CrossRef], [Google Scholar], [Publisher]
[33]. Samuel, S.O.. Frank M., Lagbegha E., Ogherohwo E.P., Ekpekpo A., Zhimwang J.T., Ikhioya I.L., *East Eur. J. Phys*., 2023, **1**:189 [CrossRef], [Google Scholar], [Publisher]
[34]. Reddy K.T.R., Prathap P., Miles R.W., Thin films of tin sulphide for application in photovoltaic solar cells in Photovoltaic. In: Tanaka H, Yamashita K (eds) Photovoltaics: developments, applications and impact. Nova Science, New York, 2010, pp 1–27 [Google Scholar], [Publisher]
[35]. Thangaraju B. *Thin Solid Films*, 2002, **402**:71 [CrossRef], [Google Scholar], [Publisher]
[36]. Amma D.S.D., Vaidyan, V.K., Manoj P.K., *Mater. Chem. Phys.*, 2005, **93**:194 [CrossRef], [Google Scholar], [Publisher]
[37]. Deshpande N.G., Vyas J.C., Sharma R. *Thin Solid Films*, 2008, **516**:8587 [CrossRef], Google Scholar], [Publisher]
[38]. Manivannan P., Subrahmanyam A., *J. Phys. D: Appl. Phys.*, 1993, **26**:1510 [Google Scholar]
[39]. Shamala K.S., Murthy L.C.S., Narasimha R.K. *Bull. Mater. Sci.*, 2004, **27**:295, [CrossRef], [Google Scholar], [Publisher]
[40]. Mahmood S.S., Atiya A.J., Abdulrazzak F.H., Alkaim A.F., Hussein F.H. *J. Med. Chem. Sci*., 2021, **4**:225 [CrossRef], [Google Scholar], [Publisher]

How to cite this manuscript: Egwunyenga N. Josephine, Okunzuwa S. Ikponmwosa, Thamer Alomayri, Imosobomeh L. Ikhioya. Enhanced physical properties of SnS/SnO semiconductor material. *Journal of Medicinal and Nanomaterials Chemistry*, 2023, 5(3), 199-212. DOI: 10.48309/JMNC.2023.3.3